JOURNAL OF Materials CHEMISTRY

Salted mesostructures: salt–liquid crystal templating of lithium triflate–oligo(ethylene oxide) surfactant–mesoporous silica nanocomposite films and monoliths

Ömer Dag,[a] Atul Verma,[a] Geoffrey A. Ozin*[a] and Charles T. Kresge[b]

[a]*Material Chemistry Research Group, Lash Miller Chemical Laboratories, University of Toronto, 80 St. George St, Toronto, Ontario, M5S 3H6 Canada*
[b]*Mobil Technology Company, Paulsboro, New Jersey 08066–0480, USA*

Received 4th February 1999, Accepted 26th March 1999

A lyotropic lithium triflate–silicate liquid crystal is utilized as a supramolecular template for a 'one-pot' synthesis of a novel ionically conducting nanocomposite material, denoted meso-SiO_2–$C_{12}(EO)_{10}OH$–$LiCF_3SO_3$, in the form of a film or monolith. In this structure Li^+ ions interact, in a crown ether-like fashion, with oligo(ethylene oxide) head groups of a non-ionic surfactant assembly that is imbibed within the channels of hexagonal mesoporous silica. Details of the acid catalyzed polymerization of the silicate oligo(ethylene oxide) surfactant co-assembly in the presence of lithium triflate have been investigated using polarized optical microscopy (POM), powder X-ray diffraction (PXRD), multinuclear nuclear magnetic resonance (NMR) spectroscopy and impedance spectroscopy. Insight into the incorporation of Li^+ and $CF_3SO_3^-$ ions into meso-SiO_2–$C_{12}(EO)_{10}OH$–$LiCF_3SO_3$ was obtained using NMR and Fourier transform (FT) Raman spectroscopy. Collectively the results indicate that lithium ions coordinate to oxygens of the oligo(ethylene oxide) head group, maintain the structural integrity of both the silicate liquid crystal and templated mesoporous silica, and are essentially completely dissociated with respect to the triflate counteranion. ac Impedance spectroscopy, which bodes well for their use in the fields of polymer electrolytes and battery technology for meso-SiO_2–$C_{12}(EO)_{10}OH$–$LiCF_3SO_3$ have demonstrated high ionic conductivities at room temperature measurements. Salt–liquid crystal templating may offer a general approach for synthesizing diverse kinds of salted mesostructures including redox active transition metal complexes, which may be reductively-agglomerated to form metal cluster-based meso-SiO_2–$C_{12}(EO)_{10}OH$–M_n or sulfided with H_2S to produce semiconductor cluster-based meso-SiO_2–$C_{12}(EO)_{10}OH$–$(MS)_n$ nanocomposites.

Introduction

Power sources for electric vehicles and portable electronic equipment are contingent upon the discovery of electrochemical systems that store a large amount of energy, deliver high power, utilize lightweight materials, and can be reversibly recharged without deterioration.[1] In lithium solid state batteries, LSSB, the cathode material, for example, CoO_2, MnO_2, or V_6O_{13}, is an insertion/intercalation compound for Li^+ ions. The electrolyte is generally a Li^+ salt. A suitable solid electrolyte for LSSB should have high room temperature Li^+ ion conductivity, compatibility with lithium metal, insertion or carbon anodes, a high decomposition potential, and ease of forming a thin film. In this regard, polymer electrolytes are the newest materials to receive wide attention.[2] Unlike inorganic ceramic and glass electrolytes, polymer electrolytes like poly(ethylene oxide), PEO, are compliant which offers mechanical advantages in the construction of LSSB. A disadvantage of PEO-based electrolytes is that the room temperature conductivity is low. Batteries utilizing PEO plasticized with an organic solvent alleviate this problem, however, they pose electrolyte mechanical, electrode corrosion and safety problems.[1] Nanocrystalline metal oxide 'solid plasticizers' are beginning to show promise for surmounting these difficulties.[3]

Herein we describe a novel class of lithium triflate–oligo(ethylene oxide) surfactant-mesoporous silica-based nanocomposite materials which may prove to be of value as solid electrolytes or solid plasticizers in LSSB. In essence, a lyotropic lithium triflate-liquid crystal is utilized as a supramolecular template for a 'one-pot' synthesis of meso-SiO_2–$C_{12}(EO)_{10}OH$–$LiCF_3SO_3$, in which Li^+ ions interact in a pseudo-crown ether-like fashion with oligoethylene oxide head groups of a non-ionic surfactant assembly, $C_{12}(EO)_{10}OH$, that is imbibed within the channels of hexagonal mesoporous silica, meso-SiO_2. It is interesting to enquire whether nanocomposites having this architecture display high Li^+ ion mobilities because of envisioned favorable ion conduction pathways associated with very high surface area oligo(ethylene oxide)–mesoporous silica interfaces (*ca.* 1000 m^2 g^{-1}) in this class of materials. In the following, we briefly survey background literature that is considered pertinent to the work described in this paper.

Since the discovery of silicate liquid crystal templating of mesoporous silica MCM-41 materials, by Mobil scientists, tremendous effort has been devoted to the synthesis of other mesoporous metal oxides,[4] as well as metal sulfides[5] and metals[6] using different surfactants and precursors. In the context of the present study, non-ionic surfactants have been shown to template hexagonal, cubic and lamella forms of mesostructured silica.[7–11] One of the non-ionic surfactants employed comprises a hydrophobic alkane C_nH_{2n+1} tail and a hydrophilic oligo(ethylene oxide) $(CH_2CH_2O)_n$ head group. Hydrogen-bonding of water to the oligo(ethylene oxide) establishes the conformation of the head group while the water : surfactant ratio predicates the formation of a hexagonal, cubic or lamella mesophase.[12] Silicification of the non-ionic surfactant mesophase yields the respective mesostructured silica replica material which can display well ordered channels, pores or lamellae.[7,8]

The central tenet of the present study is that ethylene oxide units also exist in PEO which is one of the most promising candidates for LSSB.[13–15] Dissociation of $LiCF_3SO_3$ in PEO, where the ethylene oxide units are housing the conducting Li^+ ions, has been widely studied.[13–15] Strong crown ether-like interactions between CH_2CH_2O units and Li^+ ions create resistivity which is believed to originate from constrained segmental motion of the polymer chain. Resistive dynamics of the polymer–salt electrolyte can be mediated by introducing

nanocrystalline metal oxides that function as 'solid plasticizers'.[3] It is believed that surface interactions, involving the polymer and anions with the nanocrystallites, serve to stabilize a glassy polymer structure at room temperature, which facilitates motion of the Li^+ ions while retarding that of the anions. These effects are manifest as a substantial increase of the transport number of Li^+ cations relative to X^- counter anions and enhancement of the room temperature ionic conductivity of Li^+. The salt of choice is usually lithium triflate $LiCF_3SO_3$ because it has a high solubility in PEO and moreover the triflate $CF_3SO_3^-$ anion is essentially non-coordinating with respect to the PEO. Further, numerous detailed studies of the dissociation of $LiCF_3SO_3$ in PEO with different molecular weights have been reported.[13–15] In particular one learns that free ions, ion-pairs and ion-aggregates of Li^+ and $CF_3SO_3^-$ are conveniently identified using Raman spectroscopy.[13–15]

Experimental

Synthesis

2.0 g of the non-ionic surfactant $CH_3(CH_2)_{11}$-$(CH_2CH_2O)_{10}OH$, denoted $C_{12}(EO)_{10}OH$, is added to a mixture of 2.40 g of H_2O, 0.12–1.0 g of lithium triflate, $LiCF_3SO_3$ and 0.14 g of nitric acid, HNO_3, to form a viscous gel. A clear hexagonal LC phase, seen by the characteristic fan optical birefringence texture in the POM, is obtained by homogenizing the gel at 70–80 °C at which point 2.86–3.70 g of tetramethylorthosilicate, TMOS, is added. Hydrolysis of the TMOS causes loss of structure of the hexagonal LC phase as signalled by POM. The methanol hydrolysis product is slowly removed from the mixture by applying a gentle vacuum. During this procedure the solution bubbles for few minutes. When bubbling stops the resulting fluid is poured onto a glass microscope slide to form a viscous film. Silicification of the film is also readily followed by POM. Over a silicification period of 10–60 min one observes the gradual re-establishment of the characteristic fan texture of the hexagonal LC but now it is rigidified in the form of a hexagonal mesoporous silica film. Depending on the choice of synthesis conditions, particularly the acidity and temperature, the condensation–polymerization of the silicate mesophase can progress over hours to days but never appears to reach completion (based on ^{29}Si MAS NMR $Q_n(SiO)_{4-n}(OH)_n$ ratios, see later). This synthesis paradigm (Fig. 1) has been generalized to include other main group salts as well as transition metal complexes. Details of this extension will be reported elsewhere.

Instrumentation

Polarized optical microscopy (POM) images were recorded in transmission mode on an Olympus BH-2 microscope using convergent white light between parallel and crossed polarizers. Powder X-ray diffraction (PXRD) patterns were obtained on a Siemens D5000 diffractometer using a high power Cu-Kα source operating at 50 kV/35 mA. FT-Raman spectra were recorded from samples on an Al plate using a Bomems MB-157 FT-Raman spectrometer with an InGaAs near-IR detector. The light source is a Spectra Physics diode pumped Nd:YLF laser emitting at 1064 nm with a 350 kHz repetition rate. Notch filters covering 150–3750 cm^{-1} were used to block the Rayleigh scattering. The instrument was configured in 180° back scattering mode. Samples were placed in sealed glass capillary tubes. Magic angle spinning nuclear magnetic resonance (MAS NMR) spectra were recorded on samples packed into 4 mm zirconium rotors using a Bruker DSX 400 spectrometer. The samples were spun at 8–10 kHz, all chemical shift values are reported with respect to tetramethylsilane and the following experimental parameters were employed: ^1H MAS NMR single pulse experiment, recycle delay time of 1.0 s, $\pi/2$ pulse width of 4.0 μs, 8 scans, spinning speed 8 kHz and referenced to TMS. ^{13}C MAS NMR proton high power decoupling experiment, recycle delay time of 10 s, $\pi/2$ pulse width of 5.50 μs, spinning speed of 8 kHz, 2000–5000 scans and referenced to TMS. $^{29}Si/^1H$ MAS NMR single pulse experiment, recycle delay time of 120 s, $\pi/2$ pulse width of 5.75 μs, spinning speed 8 kHz, 450 scans and referenced to TMS. ^7Li MAS NMR single pulse experiment, recycle delay of 5 s, $\pi/2$ pulse width of 2 μs, spinning speed of 10 kHz, 350–450 scans and referenced to LiCl. Transmission electron microscopy (TEM) images were obtained using a Philips 430 microscope operating at an accelerating voltage of 100 kV. The samples were embedded in epoxy resin and sectioned using an RMC MT600 ultramicrotome in combination with a Drukker diamond knife using the standard procedure. Ionic conductivity measurements were carried out using impedance spectroscopy. Samples for electrical measurements were prepared from pristine powders by pressing them into a Macor sample holder. The separation between platinum electrodes was of the order of 2.0 mm, while the cross sectional area was 4×4 mm. Samples were placed in a stainless steel chamber equipped with vacuum pump and DC heater. The samples were subjected to a dynamic vacuum of 10^{-2} Torr. Direct current was used for the heater in order to minimize interference with the impedance measurements. A K-type thermocouple was placed close to the sample and they were allowed to equilibrate for 2 h at each temperature steps. ac Impedance data were acquired using a Solartron Frequency Response Analyzer Model 1260 in the frequency range of 1 Hz to 1 MHz. The ac excitation amplitude was 10 mV. Nulling files were used to minimize parasitic effects due to sample leads and holder. Automated acquisition was facilitated by ZPLOT Version 2.1a (Scribner Associates) software. Analysis of the acquired impedance spectrum was performed using ZVIEW Version 1.5 (Scribner Associates). Ionic conductivities were calculated using relation (1)

$$\sigma_i = \frac{1}{R_i} \frac{sample\ thickness}{cross\ sectional\ area} \quad (1)$$

R_i was deduced from the intercept of the left semi-circle (*i.e.* high frequency relaxation) on the *x*-axis, see later.[16,17]

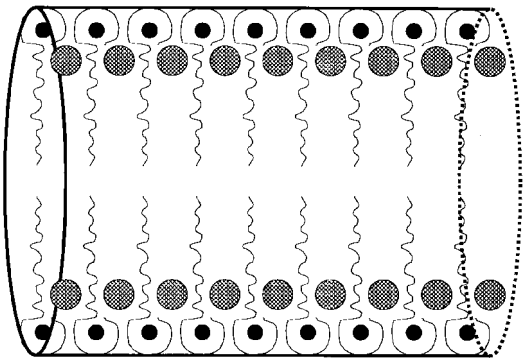

Fig. 1 Graphical representation of the paradigm 'salt-liquid crystal templating'. In a 'one-pot' synthesis, a lithium triflate–silicate–oligo-(ethylene oxide) surfactant mesophase, in the form of a thin film, undergoes an acid catalyzed polymerization to generate a lithium triflate–silicate–oligo(ethylene oxide) surfactant–mesoporous silica nanocomposite film. The $LiCF_3SO_3$ is found to be dissociated into free lithium (small solid black circle) and triflate (large hatched circle) ions in the oligo(ethylene oxide) head group region of the surfactant assembly (thin black lines) that is imbibed within the channels (thick black line) of the mesoporous silica. The nanocomposite material is a fast lithium ion conductor at room temperature which bodes well for this new class of materials finding utility in the important field of polymer electrolyte and battery technology.

Results

The hexagonal LC phase formed by surfactant and water is preserved during the silicification of the TMOS precursor. The process was conveniently monitored by *in situ* POM, PXRD, FT-Raman and NMR techniques. A synthesis mixture was transferred onto a glass slide where the POM images were recorded as a function of time. An initially optically isotropic mixture of the water, surfactant, salt, acid and silica source is seen to gradually transform into an optically anisotropic fan texture upon evaporation of the CH_3OH that is evolved during hydrolysis of TMOS[7] (Fig. 2). In the early stages of the silicification the viscous hexagonal LC phase can be used to coat a substrate or fill a shaped vessel. Upon rigidification the resulting monolithic mesoporous silica essentially preserves the original form of the viscous film or shape. The monoliths are optically transparent and in a form that makes them amenable to a wide range of characterization methods.

PXRD patterns were recorded on both film samples prepared on glass microscope slides and powdered film samples. Film samples made on glass slides display very intense and narrow 100 and 200 reflections (Fig. 3). Usually the first peak is so intense that without adequate precaution it can damage the X-ray detector and is not usually recorded. TEM shows that mesoporous silica samples prepared on glass microscope slides appear to have their channels oriented parallel to the surface of the substrate (Fig. 3 and 4).

FT-Raman spectra clearly reveal fingerprint modes of $CF_3SO_3^-$ ions in the samples and establish that free ions and ion-pairs co-exist in meso-SiO_2–$C_{12}(EO)_{10}OH$–$LiCF_3SO_3$ samples with an intensity ratio of around 3 : 1 (Fig. 5 and 6).

Nuclear magnetic resonance and vibrational spectroscopy provided powerful probes of local structure, bonding and dynamics for Li^+–surfactant assemblies either in the pristine state or imbibed within the channels of the mesoporous silica matrix. To amplify, ^1H and ^{13}C MAS NMR spectra of the pristine surfactant, $LiCF_3SO_3$–surfactant and meso-SiO_2–$C_{12}(EO)_{10}OH$–$LiCF_3SO_3$ show dramatic changes in the FWHM of surfactant related resonances (Fig. 7–9). Broadening of resonances associated with the EO units is much greater than those of alkane chain carbons and protons. ^1H MAS NMR spectra of meso-SiO_2–$C_{12}(EO)_{10}OH$–$LiCF_3SO_3$ display diagnostic resonances of surfactant as well as one at δ *ca.* 5.2–5.8 thought to be due to water and/or hydroxonium (Fig. 7 and 8). ^7Li MAS NMR spectra of meso-SiO_2–$C_{12}(EO)_{10}OH$–$LiCF_3SO_3$ display very narrow resonances compared to solid $LiCF_3SO_3$ and $LiCF_3SO_3$ incorporated into PEO (Fig. 10). ^{29}Si MAS NMR spectra of meso-SiO_2–$C_{12}(EO)_{10}OH$–$LiCF_3SO_3$ display peaks at $\delta -91(Q_2)$, $-101(Q_3)$ and $-110(Q_4)$ with respect to tetramethylsilane (TMS) with an intensity ratio that varies with aging of the samples (Fig. 11). The ^{29}Si MAS NMR spectra of samples polymerized for 1 day, 5 days, 1 month and 2 months display increasing intensity of the Q_4 resonance.

Impedance spectra exhibited by meso-SiO_2–$C_{12}(EO)_{10}OH$–$LiCF_3SO_3$ are shown in Fig. 12 and 13. Two distinct processes are noticeable in the impedance spectra. The high frequency relaxation is ascribed to the faster process of Li^+ ion conduction in the bulk, while the incomplete low frequency relaxation is most probably due to the electrodes. The ac impedance data is modeled as a electrical circuit which involves a connection of two *RC* circuits in series.

Discussion

POM is a very informative technique for monitoring the polymerization and analyzing the quality of silicified liquid crystal materials.[7] The surfactant–water (50 w/w%) mixture shows a classic hexagonal LC fan optical birefringence texture between crossed polarizers.[7,12] The surfactant/water LC phase does not alter with addition of $LiCF_3SO_3$ and HNO_3. The thermal properties of the mixture of surfactant/water, salt and acid were studied between crossed polarizers using optical microscopy. Representative POM images of the $LiCF_3SO_3$ system before and after the addition of the TMOS silica source are shown in Fig. 2. It is worth noting that the liquid crystal to isotropic liquid phase transition does shift to higher temperature with increasing salt concentration.

Addition of TMOS to the surfactant/water/salt/acid hexagonal LC yields an isotropic fluid which is believed to result from disruption of the LC structure by TMOS and/or evolved methanol. Gentle removal, by evacuation, of methanol evolved upon hydrolysis of TMOS from the reaction mixture yields a much thicker solution which remains isotropic for 10–60 min. Further evaporation of methanol and polymerization of silicate facilitate reorganization of the hexagonal LC phase. This is visualized by the appearance of the diagnostic POM fan texture first in the edge regions of the film on the glass slide, which gradually spreads to cover the entire sample in *ca.* 10 min. At this stage the LC phase is still soft and can be easily disrupted upon heating. The texture of the hexagonal phase is retained throughout the duration of a synthesis provided it is maintained at room temperature. It is important to note the exceptional sensitivity of the organization of this system to small changes of temperature. At 30 °C the system becomes isotropic and at lower temperatures it is anisotropic—low temperature self-assembly at 10–20 °C is an aspect for further investigation.

PXRD patterns of meso-SiO_2–$C_{12}(EO)_{10}OH$–$LiCF_3SO_3$ samples prepared on glass microscope slides display a very intense 100 reflection with a *d*-spacing of 46 Å and a hexagonal unit cell parameter *a* of 65 Å. Only the 200 reflection is shown for three samples with increasing Li^+ ion content, Fig. 3(A).

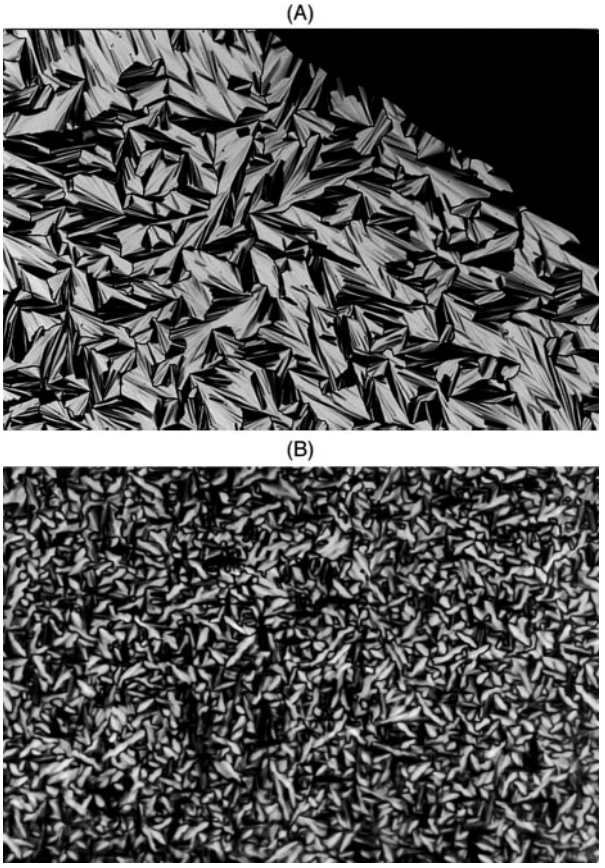

Fig. 2 POM images between crossed polarizers of (A) mesophase of surfactant $C_{12}(EO)_{10}OH$, water, nitric acid and $LiCF_3SO_3$ and (B) meso-SiO_2–$C_{12}(EO)_{10}OH$–$LiCF_3SO_3$ material obtained from the mesophase in (A) after reaction with TMOS.

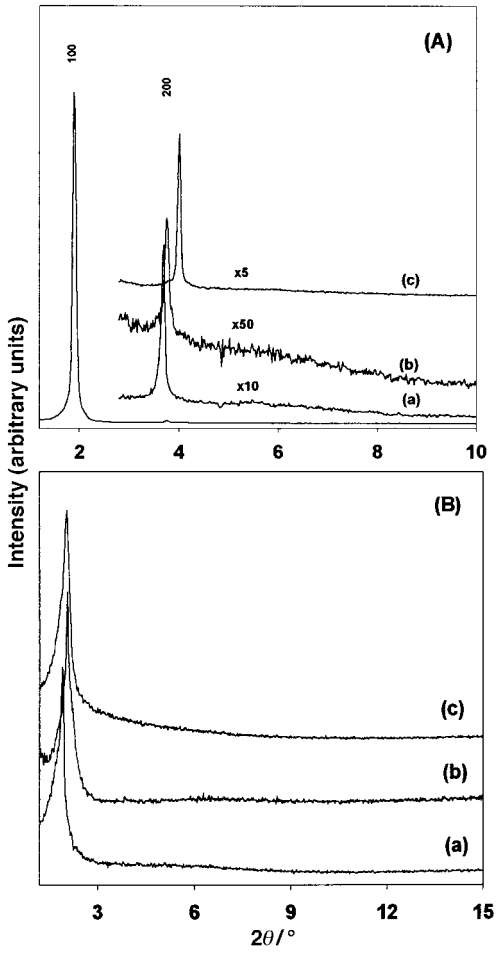

Fig. 3 PXRD patterns of as-synthesized meso-SiO_2–$C_{12}(EO)_{10}$-OH–$LiCF_3SO_3$ materials. (A) Oriented samples prepared on glass microscope slides with (a) 0.12, (b) 0.31 and (c) 0.62 mol equivalents of $LiCF_3SO_3$ per surfactant molecule. (B) Ground film samples (a) from glass microscope slides, (b) washed sample and (c) grown on plastic trays.

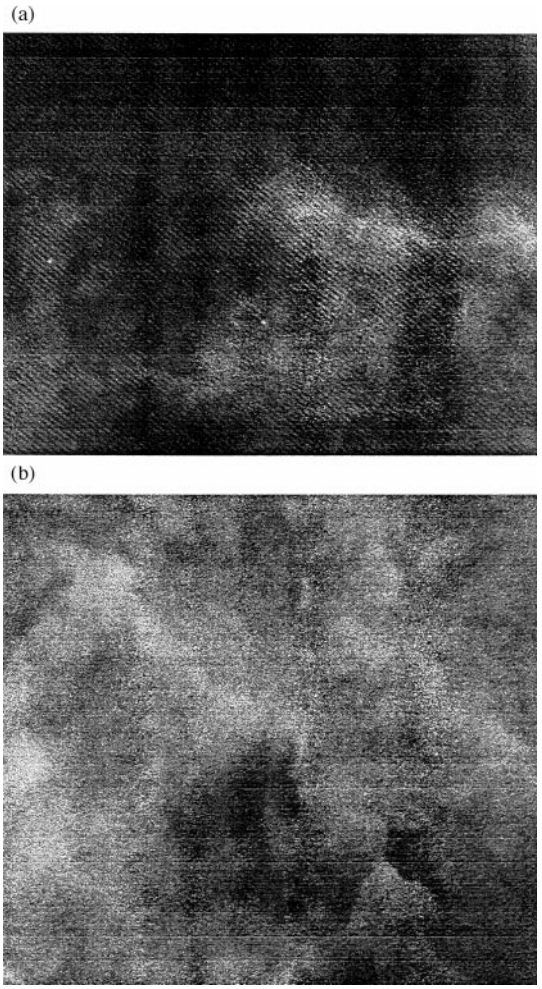

Fig. 4 TEM image of (A) ordered (scale bar: 50 nm) and (B) disordered (scale bar: 60 nm) meso-SiO_2–$C_{12}(EO)_{10}OH$–$LiCF_3SO_3$ materials synthesized on glass microscope slides (A) and ground to a powder (B).

The 100 reflection is usually *ca.* 60 times more intense than the 200. This observation and the absence of 110 and 210 reflections implies that there is preferred orientation of the channels parallel to the surface of the glass substrate. Similar effects have been reported for oriented films of mesoporous silica synthesized under quiescent, acidic aqueous conditions at water/air,[18] water/graphite[19] and water/mica interfaces.[20] By contrast, ground-up meso-SiO_2–$C_{12}(EO)_{10}OH$–$LiCF_3SO_3$ film samples only display a broad and less intense 100 reflection with a *d*-spacing around 44–50 Å, Fig. 3(B). This indicates that a well ordered and oriented film of meso-SiO_2–$C_{12}(EO)_{10}OH$–$LiCF_3SO_3$, which is known from NMR to be incompletely polymerized following a room temperature acidic synthesis, can have the mesostructure disrupted by mechanical grinding, as seen in the less organized powdered film meso-SiO_2–$C_{12}(EO)_{10}OH$–$LiCF_3SO_3$ sample. Confirmation of the PXRD results stems from TEM images that have been recorded for the film and powdered film samples, Fig. 4(A). The meso-SiO_2–$C_{12}(EO)_{10}OH$–$LiCF_3SO_3$ film shows rather well ordered mesopores in the TEM image with a *d*-spacing of about 42 Å whereas the powdered film sample is not sufficiently organized to give a clearly resolved image of the mesopores, Fig. 4(B).

Raman spectroscopy has been widely used to characterize the nature of $LiCF_3SO_3$ in PEO[13] and PPO.[14,15] It is well documented that the $\nu(SO_3)$ mode of the triflate ion is an excellent probe for monitoring structure and dynamics of Li^+ ions in polymers. To expand upon this approach, the Raman spectrum of solid $LiCF_3SO_3$ displays a peak at 1079 cm^{-1} corresponding to the $\nu(SO_3)$ symmetric stretching mode which red-shifts by 45 cm^{-1} to 1033 cm^{-1} in the free ion. Diagnostic Raman modes of the ion pair occur around 1049 cm^{-1} with aggregates around 1059 cm^{-1}.[13–15] The $LiCF_3SO_3$ salt is very hygroscopic and is able to absorb water from air to form a solution in a couple of hours. The Raman spectrum of a saturated solution of $LiCF_3SO_3$ is quite distinct to the solid form. In particular, the $\nu(SO_3)$ mode appears at 1069 cm^{-1} which is even more shifted than that of the aggregates observed in PEO and PPO, and most likely originates from higher nuclearity aggregates.

The Raman active $\nu(SO_3)$ mode was also found to be a useful probe of Li^+ ions in meso-SiO_2–$C_{12}(EO)_{10}$-OH–$LiCF_3SO_3$. The O : Li^+ concentration range investigated in this study is from 80 : 1 to 10 : 1 which is equivalent to 0.125 to 1.0 $LiCF_3SO_3$ per oligo(ethylene oxide) surfactant molecule. Fig. 5 shows the Raman spectra of four samples with increasing $LiCF_3SO_3$ concentration with the spectrum of solid lithium triflate salt included for the purpose of comparison. It is clear that the peak at 1047 cm^{-1} due to ion-pairs gradually increases with lithium triflate concentration. The FT-Raman spectra display the peak at 1035 cm^{-1} in samples containing $LiCF_3SO_3$ showing the existence of Li^+ ions free of interaction with triflate. A question that arises is whether the dissociation is due to solubility of $LiCF_3SO_3$ in the surfactant or in water present in the samples. The Raman spectra of dried samples (prepared with Li^+ : surfactant ratio of 0.31 : 1.0 and 0.68 : 1.00, pumped 10^{-5} Torr, heated for 1 h from room temperature to

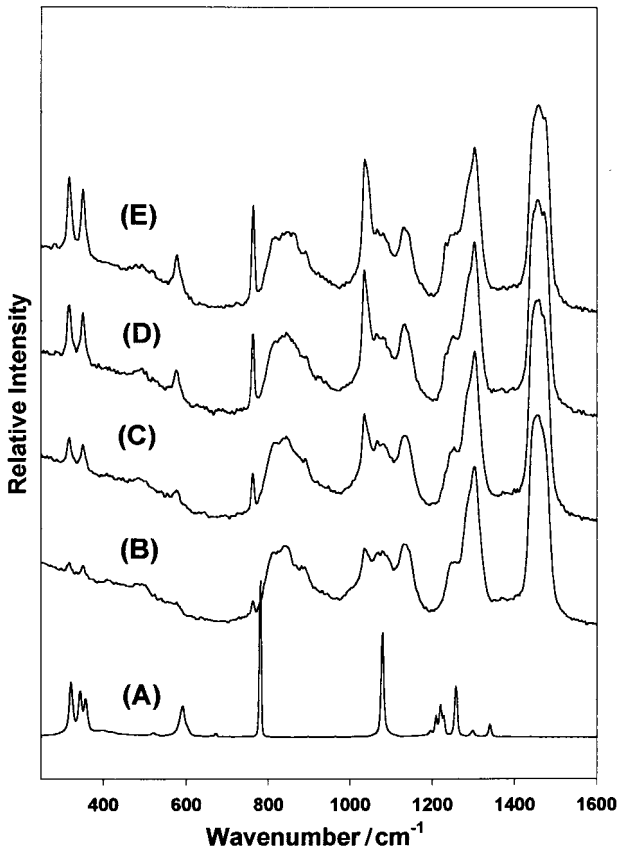

Fig. 5 FT-Raman spectra of meso-SiO_2–$C_{12}(EO)_{10}OH$–$LiCF_3SO_3$ with different mol equivalents of $LiCF_3SO_3$ per surfactant molecule in the synthesis mixture: (A) solid $LiCF_3SO_3$ and (B) 0.12, (C) 0.31, (D) 0.62 and (E) 0.78.

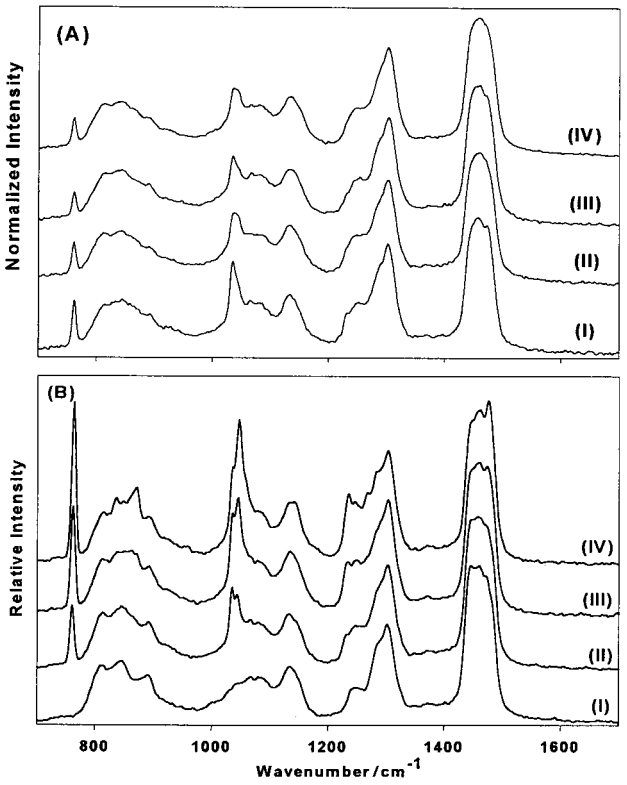

Fig. 6 FT-Raman spectra of (A) as-synthesized and vacuum dried samples of meso-SiO_2–$C_{12}(EO)_{10}OH$–$LiCF_3SO_3$ with 0.62 $LiCF_3SO_3$ per surfactant molecule (I) and (II), respectively, and of meso-SiO_2–$C_{12}(EO)_{10}OH$–$LiCF_3SO_3$ with 0.31 $LiCF_3SO_3$ per surfactant molecule (III) and (IV), respectively. (B) Dry mixture of $LiCF_3SO_3$: surfactant ratio of (I) 0, (II) 0.5, (III) 1.0 and (IV) 1.5. showing the increase of the peak due to lithium–triflate ion-pairs with the concentration of lithium triflate.

100 °C, 2 h at 100 °C) are also recorded to find the origin of the Li^+ dissociation. Fig. 6(A) displays the spectra of the as-synthesized and dried samples. It is clear from the $\nu(SO_3)$ modes that the $CF_3SO_3^-$ anions are still in the free ion state, but due to disordering of the surfactant head group in the mesoporous silica channels, the $\nu(SO_3)$ modes are broadened. The FWHM of the main peak at 1035 cm^{-1} increases from 14 cm^{-1} in the as-synthesized sample to 20 cm^{-1} in the vacuum dried samples. The inhomogeneous broadening of the surfactant Raman mode will be further discussed in the ^1H MAS NMR section. The apparent decrease in intensity of the 1035 cm^{-1} Raman band is most likely due to this broadening. Samples prepared with $O:Li^+$ ratios of 40:1, 20:1, 10:1 and 5:1 were also prepared without acid and with a surfactant to water ratio of 50:50 w/w%. These samples display surfactant and free triflate anion peaks. The only change from 5:1 to 40:1 is that the peaks due to triflate ion become more intense and broader. Over this concentration range only the free triflate ion peak is seen at 1035 cm^{-1}. However, for the sample prepared with no water it is found that peaks due to ion pairs and aggregates are observed at higher salt concentrations 30:1, 20:1 and 10:1. It is clear that at higher concentrations of lithium triflate the peak due to the ion pair increases leaving the intensity of the free ion essentially constant, Fig. 6(B). Clearly there is an equilibrium between the ion pairs and the free ions in this system. Together these results suggest that the dissociation of lithium triflate is quite high in both the pristine surfactant and the surfactant imbibed within the channels of the meso-SiO_2–$C_{12}(EO)_{10}OH$–$LiCF_3SO_3$ nanocomposite material.

^1H, ^{13}C, ^7Li and ^{29}Si MAS NMR spectra of lithium triflate incorporated samples have been recorded in order to probe local structural detail concerning surfactant, lithium and triflate ions in the mesoporous silica material. ^1H MAS NMR spectra of samples containing different amounts of $LiCF_3SO_3$ salt are displayed in Fig. 7. The spectrum of free surfactant $C_{12}(EO)_{10}OH$ displays peaks at δ 3.60 and 3.43 due to CH_2 groups of the EO units, δ 1.55 and 1.32 due to CH_2 groups of the alkyl chain, and δ 0.93 due to the CH_3 end group of the alkyl chain (referenced to TMS). Relatively broad versions of these same peaks are observed for $C_{12}(EO)_{10}OH$ in the mesoporous silica samples. Peaks due to EO units are much broader than those of the alkyl chain due to interaction of EO with the silica surface of the channels. Increasing Li^+ concentration in the meso-SiO_2–$C_{12}(EO)_{10}OH$–$LiCF_3SO_3$ material has little effect on the position and FWHM of the main peaks. A new peak is however observed in the meso-

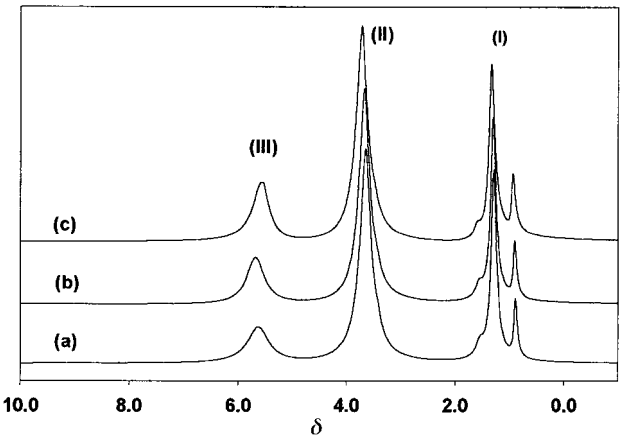

Fig. 7 ^1H MAS NMR spectra of the meso-SiO_2–$C_{12}(EO)_{10}OH$–$LiCF_3SO_3$ samples with a $LiCF_3SO_3$ to surfactant ratio of (a) 0.12, (b) 0.31 and (c) 0.62.

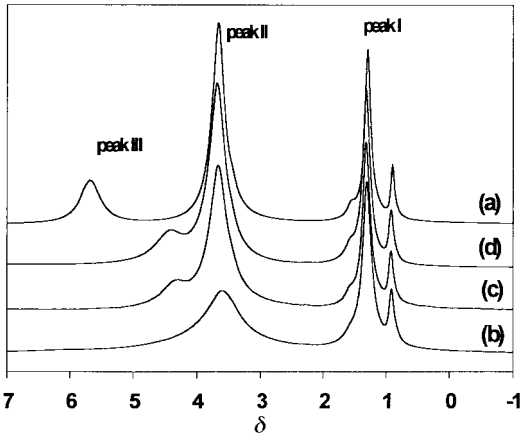

Fig. 8 ^{1}H MAS NMR spectra of the meso-SiO_2–$C_{12}(EO)_{10}OH$–$LiCF_3SO_3$ samples with $LiCF_3SO_3$ to surfactant ratio of 0.31 (a) as synthesized, (b) vacuum dried (see text), (c) vacuum dried and exposed to air for 2 days, and (d) vacuum dried and exposed to air for 12 days.

SiO_2–$C_{12}(EO)_{10}OH$–$LiCF_3SO_3$ samples around δ 5.27–5.86 likely due to imbibed water and/or hydroxonium. To clarify this point, the ^{1}H MAS NMR spectra were recorded for as-synthesized samples dried for 1 h from room temperature to 100 °C, 2 h at 100 °C under vacuum of 10^{-5}–10^{-6} Torr, as well as the dried sample subsequently exposed to air for 2 and 12 days, Fig. 8. The peak at δ 5.65 observed for as-synthesized samples disappears upon drying and the peak at δ 3.70 due to EO shifts to δ 3.60, broadens and loses intensity. The spectrum of this sample does not change much on exposure to air, however after 2 days a peak reforms at around δ 4.35 and gradually shifts to δ 4.40 in 12 days. Since the peak emerges on hydration at δ 4.40 and not δ 5.50, this indicates that evacuation removes nitric acid plus water from the samples which upon exposure to air does not return to its original structure, Fig. 8. Clearly water–surfactant–silica interactions play an important structuring role in these meso-SiO_2–$C_{12}(EO)_{10}OH$–$LiCF_3SO_3$ nanocomposite materials.

Peak area measurements show that the δ 5.60 signal (peak III) is very sensitive to the Li^+ ion and acid concentration as well as order/disorder in the head group region of the surfactant. To amplify upon this point, increasing the acid concentration shifts peak III up to δ 6.00 and to δ 5.27 in the disordered samples. The area under peak III is about 14–20% of the total area of the overall spectrum providing an estimate of 5–7 H_2O per surfactant. This corresponds to almost one water molecule per two EO units.

The overall picture that emerges from this analysis is that the conformation of the surfactant head group (quantified as the Israelachvili geometrical packing parameter) is determined by local hydrogen bonding to water molecules and their interaction with protons and/or Li^+ ions. Evacuation removes some imbibed nitric acid and the interaction between water and Li^+ ions appears to be weakened compared to when acid is present.

The ^{13}C NMR spectrum of the free surfactant displays peaks at δ 13.82, 22.60, 26.05, 29.26, 29.60 and 31.81 due to the alkyl chain and at δ 61.01, 70.02, 70.36, 70.82 and 72.70 due to EO units (referenced to TMS), Fig. 9. Peaks due to EO units become broader in the meso-SiO_2–$C_{12}(EO)_{10}OH$–$LiCF_3SO_3$ nanocomposite materials. No detectable difference was observed between ordered and disordered samples. The 1:3:3:1 quartet observed at δ 115.48, 118.66, 121.85 and 125.03 for $LiCF_3SO_3$ containing samples originates from $J(^{13}C–^{19}F)$ spin–spin coupling with a coupling constant $\delta_{CF}=3.48$ ppm, Fig. 9, inset (A). Note that the peak at δ 70.82 from the terminal carbon atom of the EO unit on the alkyl side of the surfactant is the one least affected while the

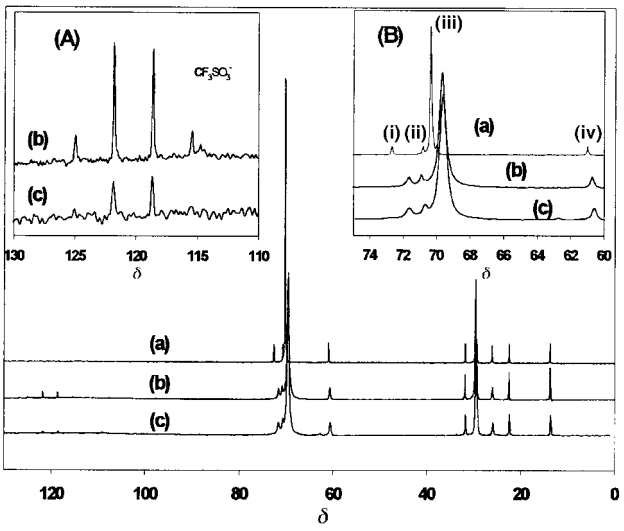

Fig. 9 ^{13}C MAS NMR spectra of (a) free surfactant, (b) meso-SiO_2–$C_{12}(EO)_{10}OH$–$LiCF_3SO_3$ material with 0.31 $LiCF_3SO_3$ per surfactant and (c) meso-SiO_2–$C_{12}(EO)_{10}OH$–$LiCF_3SO_3$ material with 0.12 $LiCF_3SO_3$ per surfactant. Inset on the left hand side (A) is the expansion of the region for triflate. Inset on the right hand side (B) is the expansion of region of EO units.

peak at δ 72.70 due to the carbon attached to the terminal OH group is the one most affected in meso-SiO_2–$C_{12}(EO)_{10}OH$–$LiCF_3SO_3$, Fig. 9, peak (i) in inset (B). This is most likely due to the fact that the OCH_2 group adjacent to the alkyl tail does not interact with either water or silica in meso-SiO_2–$C_{12}(EO)_{10}OH$–$LiCF_3SO_3$, Fig. 9, peak (ii), inset (B). By contrast, the OCH_2 group attached to the OH group most strongly interacts with the $CF_3SO_3^-$ ion. This is consistent with the FT-Raman conclusion that the solubility of $LiCF_3SO_3$ is contingent upon hydrogen-bonding of the triflate anion to the OH end group.[15] Note that the shift of this peak is *ca.* 1 ppm in samples which contain 0.31 $LiCF_3SO_3$ per surfactant, 0.85 ppm for 0.12 $LiCF_3SO_3$ per surfactant and almost zero for no $LiCF_3SO_3$. The high field shift on this peak with increasing triflate ion is consistent with the hydrogen-bonding proposal.

^{7}Li MAS NMR spectra of two $LiCF_3SO_3$ containing samples, meso-SiO_2–$C_{12}(EO)_{10}OH$–$LiCF_3SO_3$ and meso-SiO_2–PEO–$LiCF_3SO_3$ are shown in Fig. 10. Isotropic chemical shift values are referenced to LiCl. Solid $LiCF_3SO_3$ displays

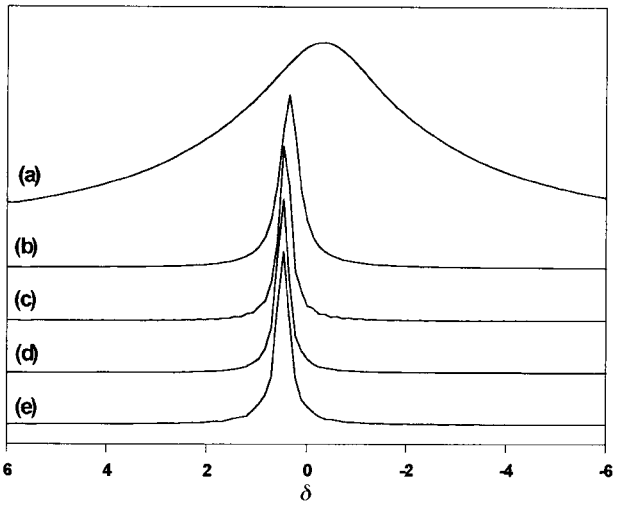

Fig. 10 ^{7}Li MAS NMR spectra of (a) solid $LiCF_3SO_3$, (b) $LiCF_3SO_3$ in meso-SiO_2–PEO–$LiCF_3SO_3$ (CH_3CN encapsulation technique), and $LiCF_3SO_3$ in meso-SiO_2–$C_{12}(EO)_{10}OH$–$LiCF_3SO_3$ with a $LiCF_3SO_3$ to surfactant ratio of (c) 0.12, (d) 0.31 and (e) 0.62.

one very broad peak at δ −0.27 while $LiCF_3SO_3$ in the mesoporous silica samples display one sharp peak at δ 0.46 with a FWHM of 0.27 ppm. The 0.70 ppm shift is most likely associated with free Li^+ ions (see FT-Raman section). Further, the narrow FWHM implies that the Li^+ ions are quite mobile in both of the mesoporous silica materials. No detectable difference was observed in the ^7Li MAS NMR spectra between ordered and disordered versions of meso-SiO_2–$C_{12}(EO)_{10}OH$–$LiCF_3SO_3$ samples, Fig. 10. This NMR observation is also consistent with the FT-Raman results implying that neither of these techniques may be able to resolve the difference between free Li^+ ions in the channels of ordered and disordered meso-SiO_2–$C_{12}(EO)_{10}OH$–$LiCF_3SO_3$ materials.

Silica polymerization in meso-SiO_2–$C_{12}(EO)_{10}OH$–$LiCF_3SO_3$ is quite interesting. It is observed that after mixing water, surfactant, nitric acid, lithium triflate and TMOS give a clear mobile solution for a few minutes. Removal of hydrolyzed methanol, by mild evacuation, yields after *ca.* 5 min a much thicker solution. This phase is still optically isotropic. In 10–60 min it transforms to a soft optically anisotropic hexagonal LC and then into a rigid solid with an essentially identical optical texture. The texture becomes much clearer and sharper with time. Samples with the sharpest optical texture give the most intense and narrow PXRD patterns. Silica polymerization was conveniently followed using ^{29}Si MAS NMR spectroscopy. To expand, meso-SiO_2–$C_{12}(EO)_{10}OH$–$LiCF_3SO_3$ samples typically display peaks at δ −91, −101 and −110 with respect to TMS due to $Si(OH)_{4-n}O_n$ units, where n is 2 (Q_2), 3 (Q_3) and 4 (Q_4), respectively, Fig. 11. In this context, the Q_4/Q_3 ratio is usually employed to establish the degree of silica polymerization. For example, samples polymerized for only 6 h show a Q_4/Q_3 ratio of *ca.* 0.5. This ratio increases to 0.64 for 5 days, 0.80 for 1 month and 0.95 for two months; the ratio increases further upon calcination at 450 °C. The Q_4 peak is considerably broader than Q_3 and Q_2 and the FWHM increases with aging. The slow increase in the Q_4/Q_3 ratio clearly shows that the silica polymerization is very slow under the synthesis conditions employed in this study.

A representative example of an ac impedance spectrum exhibited by meso-SiO_2–$C_{12}(EO)_{10}OH$–$LiCF_3SO_3$ with 0.6 Li^+ per surfactant is displayed in Fig. 12. As mentioned earlier, the impedance spectra display two distinct processes, a high frequency relaxation attributed to Li^+ ion conduction in the bulk and an incomplete low frequency relaxation likely associated with the electrodes. The ac impedance data was modeled

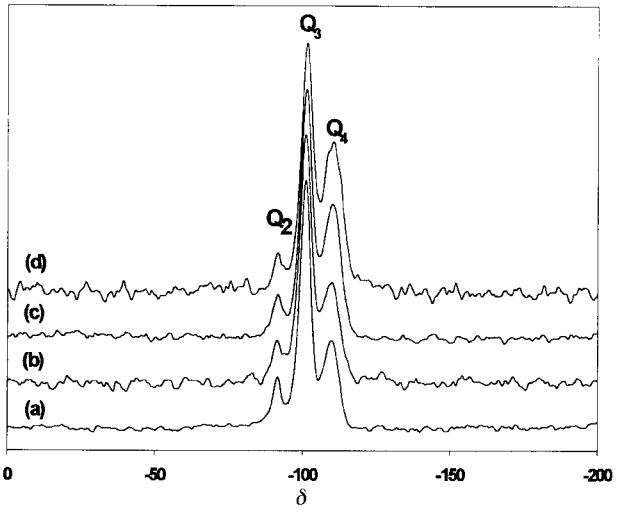

Fig. 11 ^{29}Si MAS NMR spectra showing the Q_2, Q_3 and Q_4 region of meso-SiO_2–$C_{12}(EO)_{10}OH$–$LiCF_3SO_3$ materials aged for (a) 6 h, (b) 5 days, (c) 1 month and (d) 2 months.

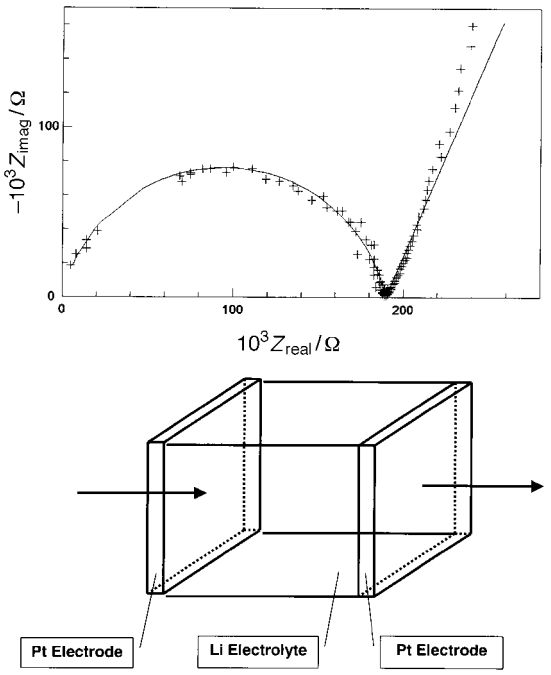

Fig. 12 (top) Impedance spectrum exhibited by meso-SiO_2–$C_{12}(EO)_{10}OH$–$LiCF_3SO_3$ with 0.6 Li^+ per surfactant. The high frequency relaxation is ascribed to Li^+ ion conduction. (bottom) Schematic of cell used for impedance measurements.

as a connection of two *RC* circuits in series and R_i was deduced from the intercept of the left semi-circle (*i.e.* high frequency relaxation) on the *x*-axis. Data of this kind was collected over a range of temperatures which enabled determination of the temperature dependence of the ionic conductivity of a collection of meso-SiO_2–$C_{12}(EO)_{10}OH$–$LiCF_3SO_3$ materials, Fig. 13. Sample II containing 0.60 Li^+ ions per surfactant shows higher measured conductivities than sample I with only 0.31 Li^+ ions per surfactant. Sample II as anticipated also exhibits enhanced conduction as temperature is increased, while sample I shows a decreasing conductivity with temperature. This behavior may be associated with loss of water and aging effects in sample I. A detailed study of ion conduction in these novel materials systems is the subject of ongoing research in this laboratory.

Conclusion

A lithium triflate–oligo(ethylene oxide) surfactant mesophase has been successfully employed in a 'one pot' synthesis of

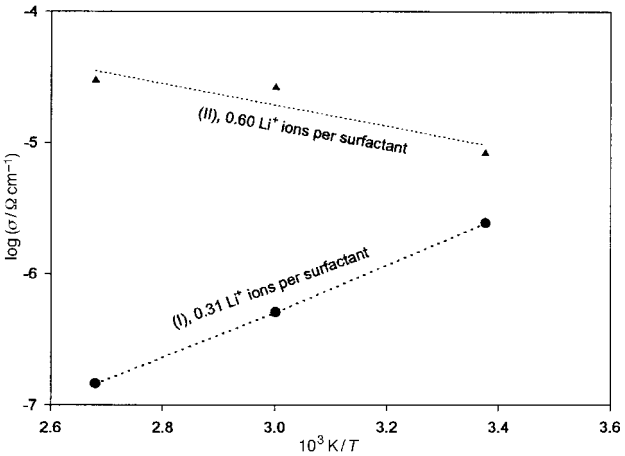

Fig. 13 Temperature dependence of Li^+ ion conduction in meso-SiO_2–$C_{12}(EO)_{10}OH$–$LiCF_3SO_3$.

meso-SiO_2–$C_{12}(EO)_{10}OH$–$LiCF_3SO_3$ nanocomposite materials in the form of a film or monolith. The $LiCF_3SO_3$ is found to be dissociated into free lithium and triflate ions in the oligo(ethylene oxide) head group region of the surfactant assembly that is imbibed within the channels of the mesoporous silica. Notably, the oligo(ethylene oxide) head groups appear to be more disordered in the absence of co-adsorbed water which may prove to be a distinctive advantage for any envisioned applications requiring high lithium ion mobility. Meso-SiO_2–$C_{12}(EO)_{10}OH$–$LiCF_3SO_3$ nanocomposites are a novel class of materials that display promising features for utility in the very important fields of polymer electrolytes and battery technology.

Acknowledgments

G.A.O. is deeply indebted to the Canada Council for the award of an Issac Walton Killam Foundation Research Fellowship (1995–97). Financial support of this work from Mobil Technology Company is deeply appreciated. The valuable assistance of Dr. Deepa Khushalani with solid state NMR and Dr. Neil Coombs with transmission electron microscopy measurements is gratefully recognized. The assistance of Mr Mark MacLachlan with the synthesis of meso-SiO_2–PEO–$LiCF_3SO_3$ samples is deeply appreciated.

References

1 P. G. Bruce, *Solid State Electrochemistry*, Cambridge University Press, Cambridge, UK, 1995.
2 T. Gerfin, M. Gratzel and L. Walder, *Prog. Inorg. Chem.*, 1997, **44**, 345.
3 F. Corce, G. B. Appetecchi, L. Persi and B. Scorsati, *Nature*, 1998, **394**, 456.
4 C. T. Kresge, M. E. Leonowicz, W. J. Roth, J. C. Vartuli and J. S. Beck, *Nature*, 1992, **359**, 710; D. M. Antonetti and J. Y. Ying *Angew. Chem., Int. Ed. Engl.*, 1996, **35**, 426; T. Sun and J. Y. Ying, *Nature*, 1997, **389**, 704.
5 T. Jiang and G. A. Ozin, *J. Mater. Chem.*, 1997, **7**, 2213.
6 G. S. Attard, P. N. Bartlett, N. R. B. Coleman, J. M. Elliott, J. R. Owen and J. H. Wang, *Science*, 1997, **278**, 838.
7 G. S. Attard, J. C. Glyde and C. G. Göltner, *Nature*, 1995, **378**, 366.
8 P. T. Tanev and T. J. Pinnavaia, *Chem. Mater.*, 1996, **8**, 2068.
9 S. A. Bagshaw, E. Prouzet and T. J. Pinnavaia, *Science*, 1995, **269**, 1242.
10 C. G. Göltner, S. Henke, M. G. Weissenberger and M. Antonietti, *Angew. Chem., Int. Ed.*, 1998, **37**, 613; P. Yang, D. Zhao, B. F. Chmelka and G. D. Stucky, *Chem. Mater.*, 1998, **10**, 2033.
11 D. Zhao, Q. Huo, J. Feng, B. F. Chmelka and G. D. Stucky, *J. Am. Chem. Soc.*, 1998, **120**, 6024.
12 D. J. Mitchell, G. J. T. Tiddy, L. Waring, T. Bostock and M. P. McDonold, *J. Chem. Soc., Faraday Trans. 1*, 1983, **79**, 975.
13 G. Peterson, P. Jacobsson and L. M. Torell, *Electrochim. Acta*, 1992, **37**, 1495.
14 A. Ferry, *J. Phys. Chem.*, 1997, **101**, 150.
15 A. Ferry and M. Tian, *Macromolecules*, 1997, **30**, 1214.
16 J. R. Macdonald, *Impedance Spectroscopy Emphasizing Solid Materials and Systems*, John Wiley & Sons, New York, 1987.
17 Zplot for Windows, Electrochemical Impedance Software, Operating Manual, Scribner Associates, Inc., Version 2.0, February 1997.
18 H. Yang, N. Coombs, I. Sokolov and G. A. Ozin, *Nature*, 1996, **381**, 589.
19 H. Yang, G. A. Ozin, I. Y. Sokolov and N. Coombs, *J. Mater. Chem.*, 1997, **7**, 1285.
20 H. Yang, A. Kuperman, N. Coombs, S. Mamiche-Afara and G. A. Ozin, *Nature*, 1996, **379**, 703.

Paper 9/00955H